Acta Cryst C STRUCTURAL CHEMISTRY
ISSN 2053-2296

Structure and optical properties of a trimetallic cobalt–molybdenum–sodium metal–organic framework

Benjamin J. Moore,[a] Jeremiah P. Tidey,[b] Craig I. Hiley[a] and Richard I. Walton[a]*

[a]Department of Chemistry, University of Warwick, Coventry, CV4 7AL, United Kingdom, and [b]Department of Physics, University of Warwick, Coventry, CV4 7AL, United Kingdom. *Correspondence e-mail: r.i.walton@warwick.ac.uk

Received 11 November 2025
Accepted 26 January 2026

Edited by I. D. Williams, Hong Kong University of Science and Technology, Hong Kong

Keywords: 3D ED; metal–organic framework; coordination polymer; solvothermal; multivariate; crystal structure.

CCDC reference: 2449088

Supporting information: this article has supporting information at journals.iucr.org/c

The crystallization of a trimetallic cobalt–molybdenum–sodium metal–organic framework, poly[μ-benzene-1,3,5-tricarboxylato-tetra-μ-oxido-cobaltmolybdenumtrisodium], UOW-10 or $[Na_3Co(MoO_4)(BTC)]_n$, is achieved by solvothermal synthesis using benzene-1,3,5-tricarboxylic acid (H_3BTC, $C_9H_6O_6$) as a ligand precursor, $Na_2MoO_4{\cdot}2H_2O$ and $Co(NO_3)_2{\cdot}2H_2O$ as metal sources, and *N*,*N*-dimethylformamide (DMF) as the solvent. 3D electron diffraction (3D ED) reveals that the structure crystallizes in the monoclinic space group $P2_1/c$, with lattice parameters of a = 9.718 (2), b = 18.250 (3), c = 6.892 (9) Å, $\alpha = \gamma = 90$, β = 96.156 (15)°, V = 1214.7 (4) Å^3 and Z = 4. The phase purity of the bulk sample was confirmed using synchrotron powder X-ray diffraction. The organic ligands form a 2D layer, where cobalt and molybdenum are found, with sodium cations located between the layers. There are four crystallographically distinct sodium sites: three exhibit a distorted octahedral coordination geometry, while the remaining site is seven-coordinate. The cobalt has trigonal bipyramidal coordination geometry and molybdenum exhibits a tetrahedral coordination geometry. Half the sodium cations in the structure forms 1D column-like motifs *via* shared oxygen edges along the crystallographic *c* axis, which are cross-linked in *b* by the cobalt and molybdenum sites *via* bridging O atoms, while the other half of the sodium cations form 2D ribbons in the *ac* plane, propagating along *c*, linked by sharing oxygen edges and faces. The optical properties of UOW-10 were investigated through the use of UV–Vis spectroscopy, showing a bandgap of 1.8 eV. Deconvolution of the features in the visible-light region reveals that four peaks are present, which can all be ascribed to the *d*–*d* transitions from the trigonal bipyramidal cobalt. By means of thermogravimetric analysis (TGA) and variable-temperature powder X-ray diffraction (VT-PXRD), it is demonstrated that the material has thermal stability to 410 °C, after which structure collapse occurs, leading to a mixture of Na_2MoO_4, CoO and Co_3Mo above 900 °C.

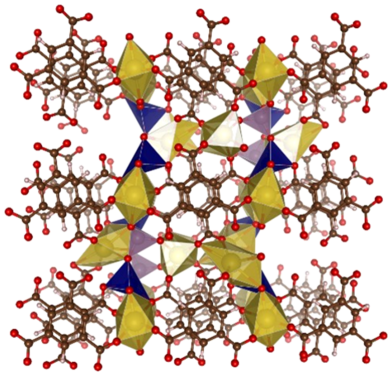

1. Introduction

In the past 30 years, metal–organic frameworks (MOFs), crystalline materials with potential porosity (Batten *et al.*, 2012) constructed from inorganic building blocks (termed secondary building units, SBUs) and organic ligands, have gained attention for their application in areas including catalysis (Wei *et al.*, 2020; Dhakshinamoorthy *et al.*, 2018; Farrusseng *et al.*, 2009), gas adsorption (Li *et al.*, 2009; Han *et al.*, 2019; Xiao *et al.*, 2025), sensing (Koo *et al.*, 2019), proton conductivity (Sharma *et al.*, 2023; Chen *et al.*, 2023) and drug delivery (Lawson *et al.*, 2021). One of the distinct advantages of MOFs in comparison to other porous materials such as zeolites is their high degree of tunability (Hao *et al.*, 2018). Systematic alterations to the metal nodes of the material or the organic linkers in the structure can result in varied properties. For example, in the field of photocatalysis, functiona-

lizing organic linkers with auxochromes such as amino, hydroxyl and aldehyde groups has been shown to be a powerful tool to modulate the absorption edge of MOFs, thereby improving photocatalytic performance (Sun *et al.*, 2013; Chambers *et al.*, 2017). In the field of gas adsorption, decoration of organic linkers with amino groups has become a common strategy to increase CO_2 adsorption capacity (Kim *et al.*, 2020).

Recently, multivariate metal–organic frameworks (MTV MOFs) have attracted attention as a means of further modulating the properties of the materials (Helal *et al.*, 2017). MTV MOFs can generally be defined as MOFs which are constructed by multiple organic ligands and/or more than one metal. This enhanced degree of tailorability has proved important in achieving high-performing materials (Castells-Gil *et al.*, 2020; Yuan *et al.*, 2016).

With regards to synthesis, MTV MOFs can be prepared either by direct crystallization under solvothermal conditions or by post-synthesis exchange of either cations or ligands. The former is exemplified by MOF-74 which can be prepared with up to ten individual metals incorporated in a one-step solvothermal synthesis, albeit with some heterogeneity in their distribution from crystal to crystal (Wang *et al.*, 2014). The latter approach may avoid the possibility of phase separation during synthesis into a mixture of crystalline phases. For example, the synthesis of mixed-linker systems, such as PCN-701, PCN-702 and PCN-703, could not be achieved from direct synthesis, but instead could only be accessed *via* a ligand installation approach (Yuan *et al.*, 2015). Here, the exploitation of the free hydroxyl groups in the low-connectivity Zr_6 cluster allows for the precise installation of two different carboxylate linkers of varying lengths, thereby increasing the connectivity of the metal cluster from eight to 12 (Yuan *et al.*, 2016).

With regards to mixed-metal systems, post-synthetic approaches have also been reported. For example, in the UiO-67–bpy system, the free N atoms in the 2,2′-bipyridine-5,5′-dicarboxylate linker can be used as sites to chelate various metals, thereby generating novel multivariate MOFs (Maza *et al.*, 2015). Another common approach is the utilization of preformed heterometallic clusters that are used as metal nodes in the construction of the MOF. For example, in PCN-415, a pre-formed $[Ti_8Zr_2O_{12}(COO)_{16}]$ is utilized as a building block to construct a novel photoactive MOF (Yuan *et al.*, 2017).

In this article, a heterometallic metal–organic framework from a readily available organic ligand is reported by a direct solvothermal reaction. The synthesis strategy was to use metal cations with distinct chemical nature. Co^{II} can be viewed as a borderline Lewis acid due to its moderate charge density, while Mo^{VI} is a hard Lewis acid due to its high charge density. The third metal, sodium, is more ionic in character, with little preferrence for coordination geometry. This difference in hardness may be interesting for applications which can benefit from mixed Lewis acidity, such as the field of catalysis (Castells-Gil *et al.*, 2020). The optical properties of the new material were measured and are strongly influenced by the cobalt coordination geometry, and thermogravimetric analysis and variable-temperature powder X-ray diffraction show the material to have good thermal stability.

Table 1
3D ED experimental details.

Crystal data	
Chemical formula	$[Na_3Co\{MoO_4\}(C_9H_3O_6)]$
M_r	494.96
Crystal system, space group	Monoclinic, $P2_1/c$
Temperature (K)	293 (5)
a, b, c (Å)	9.718 (2), 18.250 (3), 6.8892 (9)
β (°)	96.156 (15)
V (Å^3)	1214.7 (4)
Z	4
Radiation type	Electron, λ = 0.0251 Å
Collection method	Continuous rotation electron diffraction (cRED)
Probe details	2 µm diameter selected area aperture
μ (mm^{-1})	Not calculated
Data collection	
Diffractometer	Rigaku XtaLAB Synergy-ED HyPix-ED, electron source at 200 keV
No. of measured, independent and observed [$I \geq 2\sigma(I)$] reflections	3862, 3862, 3183
R_{int}	0.181
$(\sin\theta/\lambda)_{max}$ (Å^{-1})	0.626
Refinement	
$R[F^2 > 2\sigma(F^2)]$, $wR(F^2)$, S	0.182, 0.406, 1.04
No. of reflections	3862
No. of parameters	222
No. of restraints	108
H-atom treatment	H-atom parameters constrained
$\Delta\varphi_{max}$, $\Delta\varphi_{min}$ (e Å^{-1})	1.67, −1.54

Computer programs: *CrysAlis PRO* (Rigaku OD, 2025), *SHELXT* (Sheldrick, 2015), *olex2.refine* (Bourhis *et al.*, 2015) and *OLEX2* (Dolomanov *et al.*, 2009).

2. Experimental

2.1. Synthesis of $Na_3Co(MoO_4)BTC$ (UOW-10)

$Co(NO_3)_2{\cdot}2H_2O$ (87.3 mg, 0.6 mmol), $Na_2MoO_4{\cdot}2H_2O$ (72.5 mg, 0.6 mmol) and benzene-1,3,5-tricarboxylic acid (H_3BTC; 126 mg, 1.2 mmol) were added to a 25 ml Teflon-lined stainless steel autoclave, followed by 10 ml of DMF. The mixture was stirred for 1 h, then sealed and heated at 175 °C for 17 h, followed by cooling to room temperature over a period of 72 h. The resulting solid was filtered *via* a Büchner funnel and washed by pouring DMF (3 × 15 ml) over the sample, followed by drying at 70 °C in air.

2.2. Single-crystal 3D electron diffraction

Crystal data, data collection and structure refinement details are summarized in Table 1. For the 3D ED experiment, the sample was ground lightly between glass slides and dispersed dry onto a copper-supported amorphous carbon TEM grid. This was loaded at room temperature *via* a JEOL high-tilt specimen holder into a Rigaku XtaLAB Synergy-ED electron diffractometer, operated at 200 kV and equipped with a Rigaku HyPix-ED hybrid pixel array area detector. Data were collected at 293 (5) K as single-rotation scans using the

CrysAlis PRO system (Rigaku OD, 2025) for multiple crystallites appearing as microcrystalline chips using continuous rotation electron diffraction with a selected area aperture of 2 µm apparent diameter. No indication of beam damage was observed. Although data consistently indexed to the reported cell, the sample exhibited ubiquitous nonmerohedral twinning by twofold rotation about the *c* axis and, as a consequence, datasets could not be merged; data are presented for the most complete and high quality of these collections. The diffraction pattern and an image of the sample studied on the TEM grid can be seen in Fig. S1.

Data were indexed and integrated with scaling and an empirical absorption correction was applied using *CrysAlisPRO*. The structures were solved using *SHELXT* (Sheldrick, 2015) and refined using *olex2.refine* in the kinematic approximation, applying an extinction correction to broadly account for dynamical scattering, as implemented in *OLEX2* (Bourhis *et al.*, 2015; Dolomanov *et al.*, 2009), using published scattering factors (Saha *et al.*, 2022).

H atoms are placed geometrically and have positions and isotropic displacement parameters riding on their parent atoms at neutron average distances (Allen & Bruno, 2010). Non-H atoms were refined with anisotropic atomic displacement parameters and global rigid-bond restraints were employed to improve the physical sense of the displacement parameters. Experimental and refinement information are contained within the deposited CIF along with structure factors and an embedded `.res` file.

2.3. Bulk sample characterization

Powder X-ray diffraction data for phase identification were recorded on a Siemens D5000 X-ray diffractometer, using a Cu $K\alpha_{1/2}$ source producing 1.5418 Å wavelength X-rays. *In situ* powder X-ray diffraction was performed using a Bruker D8 instrument with Cu $K\alpha_{1/2}$ radiation, fitted with an Anton Paar XRK 900 chamber and a VÅNTEC solid-state detector. Samples were heated to 900 °C in flowing air and diffraction patterns were recorded at intervals of 20 °C. Room-temperature high-resolution synchrotron powder X-ray diffraction data were collected at Beamline I11 at Diamond Light Source [λ = 0.8249705 (3) Å] for structural analysis of the bulk powder. The diffraction pattern of UOW-10 was fitted to using *TOPAS 6*, with lattice parameters being the only sample parameters refined *via* the Rietveld method using the crystallographic model obtained by 3D ED (Coelho, 2018). Thermogravimetric analysis was performed using a Mettler–Toledo TGA/DSC1 under an air atmosphere with a heating rate of 5 °C. IR spectroscopy was performed on a Bruker ALPHA FT–IR ATR spectrometer, with spectra collected in the range 650–4000 cm^{-1}. Diffuse-reflectance UV–Vis spectroscopy was conducted on a Shimadzu UV-2600 spectrophotometer in the range 200–800 nm. Scanning electron microscopy (SEM) images were collected using a Zeiss SUPRA 55VP FEGSEM instrument.

3. Results and discussion

3.1. Crystal structure of UOW-10

The material crystallized at a synthesis temperature in the range 150–200 °C, as indicated by the formation of purple microcrystals, with a powder X-ray diffraction pattern consistent with the structure determination (see following). The resulting crystals were too small for laboratory or syn-

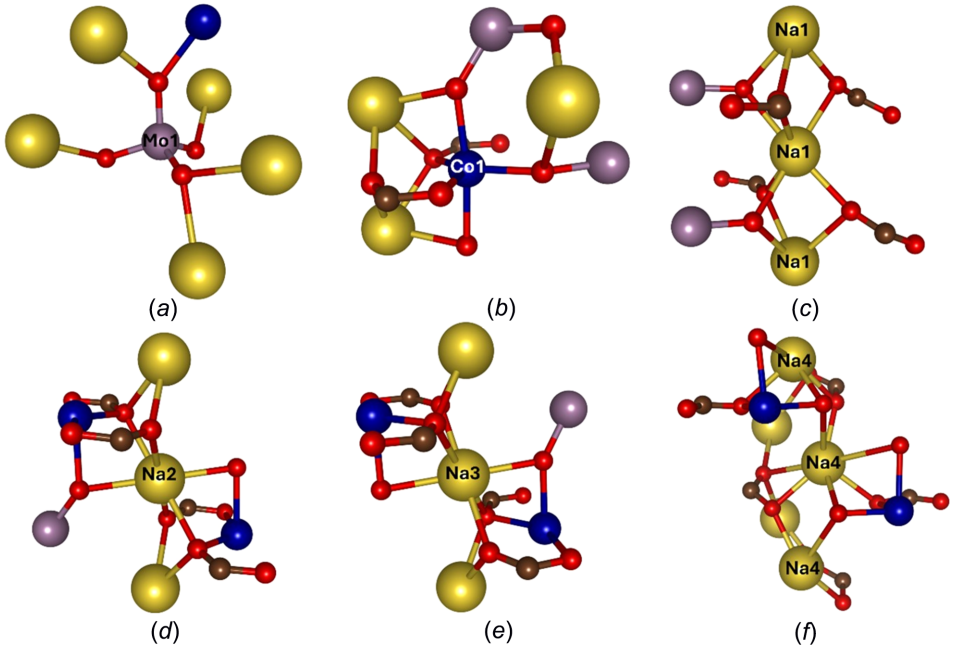

Figure 1
Local coordination environment of the atoms in UOW-10, with Co atoms shown in dark blue, Na atoms shown in yellow, Mo atoms shown in purple and O and C atoms shown in red and brown, respectively. (*a*) The Mo coordination geometry and connectivity, (*b*) the Co coordination geometry and connectivity, and (*c*)–(*f*) the Na1–Na4 coordination environments.

chrotron single-crystal X-ray diffraction (Fig. S2 in the supporting information), and so 3D ED was used to solve the structure of the material. This revealed the crystals to be a heterometallic metal–organic framework containing sodium, cobalt and molybdenum. The material, $CoMoNa_3O_4$(BTC), crystallizes in the monoclinic space group $P2_1/c$, with lattice parameters a = 9.718 (2), b = 18.250 (3), c = 6.892 (9) Å, α = γ = 90, β = 96.156 (15)°, V = 1214.7 (4) Å^3 and Z = 4. Lists of bond lengths and angles can be found in Tables S1 and S2, respectively. The molybdenum forms in a four-coordinated tetrahedral geometry and is not coordinated to the BTC linker but instead by edge-sharing oxides with cobalt and sodium [Fig. 1(*a*)]. The cobalt centres are five-coordinate with two of the equatorially coordinated O atoms resulting from a η^1-coordination of the BTC linker [Fig. 1(*b*)] and the others being oxide anions shared between cobalt, molybdenum and sodium. The Co—O bond lengths range from 1.976 (7) to 2.101 (10) Å, which is typical for Co^{II} MOFs according to the Inorganic Crystal Structure Database (ICSD, https://icsd.products.fiz-karlsruhe.de/) and the Cambridge Structural Database (CSD; Groom *et al.*, 2016). Indeed, bond valence sums suggest the oxidation state of cobalt is Co^{II} (Table S3) as opposed to Co^{III} (Brown & Altermatt, 1985).

There are four, fully occupied, crystallographically independent sodium sites, two of which are located at inversion centres in the structure. The Na1, Na2 and Na3 sites are six-coordinate, and all adopt a distorted octahedral coordination geometry. In contrast, the Na4 site is seven-coordinate. While the local connectivity of these sites vary, for all Na sites, four of the coordinating O atoms are provided by the carboxylate groups, while the remaining O atoms are oxides shared between neighbouring metal centres. For the Na1 site [Fig. 1(*c*)], the remaining oxides are shared with a molybdenum centre, for the Na2 and Na3 sites [Figs. 1(*d*) and 1(*e*)], the remaining oxides are shared with both a molybdenum and cobalt centre, and at the Na4 site, the remaining [Fig. 1(*f*)] oxides are shared between two distinct symmetry-equivalent cobalt centres.

The Na1-centred octahedra face-share with one another, thereby forming a column running along the crystallographic *c* axis. Another column running along the crystallographic *c* axis is formed by edge-sharing Na4 atoms. These two columns are interconnected by a μ_3-OCO group from the carboxylate moiety to give a double column or ribbon-like feature [Fig. 2(*a*)]. The Na2 and Na3 octahedra share edges with one another, also forming a column along the crystallographic *c* axis [Fig. 2(*b*)]. The Na2/Na3 column and Na1/Na4 double column are cross-linked by the cobalt and molybdenum sites, respectively. With regards to bond lengths, the Na—O bonds vary between 2.202 (13) and 2.908 (12) Å, which falls in the typical range for Na—O bonds according to the ICSD and CSD.

The organic ligand coordinates to several metal ions giving a complex coordination mode of the carboxylate groups [Fig. 2(*c*)]. One of the carboxylate groups binds in a μ_4:η^1:η^2:η^1:η^1 fashion to four Na sites. Another carboxylate group binds in a μ_4:η^1:η^1:η^1:η^1 fashion to three Na sites and one Co site. The final carboxylate group binds in a μ_5:η^1:η^1:η^1:η^1:η^1 fashion to four Na sites and one Co site.

Figs. 3(*a*) and 3(*b*) depict an extended views of the structure along the crystallographic *b* and *c* axes, respectively. In Fig. 3(*a*), it can be observed that all the BTC linkers are coplanar with each other connected by the Co centres, so forming layers. No free carboxylic acid groups are observed in the structure, which is in agreement with FT–IR data which show no characteristic bands of the non-ionized carboxyl groups of H_3BTC (νOH 3082 cm^{-1}; νC=O 1720 cm^{-1}). Instead, bands in the ranges 1541–1613 and 1354–1433 cm^{-1} are present, which correspond to the asymmetric COO^- and symmetric COO^- vibrations, respectively (Fig. S3) (Maiti *et*

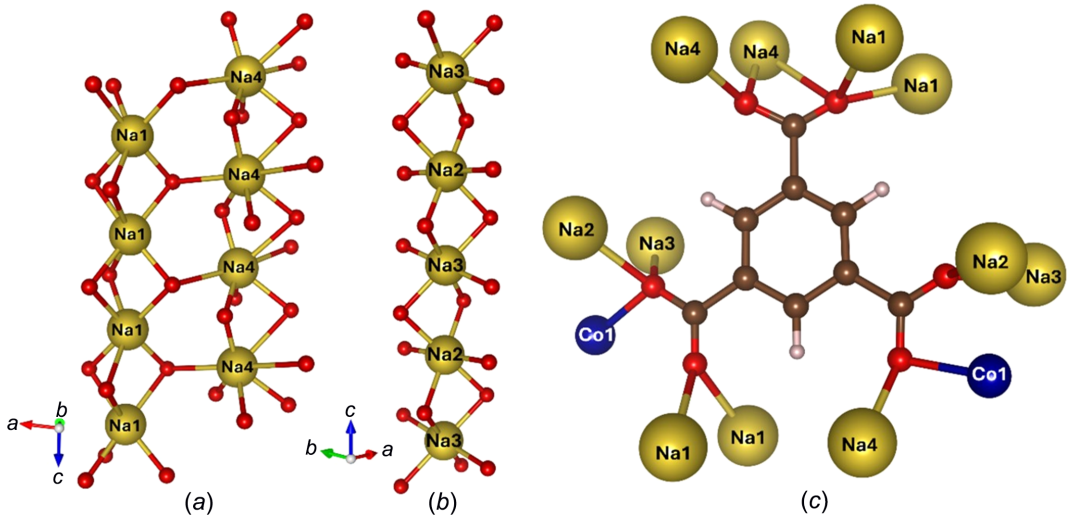

Figure 2
The structural features of UOW-10, with Co atoms shown in dark blue, Na atoms shown in yellow and O, C and H atoms shown in red, brown and white, respectively. (*a*) The Na1 and Na4 double-column ribbon running along the crystallographic *c* axis, (*b*) the Na2/3 column running along the crystallographic *c* axis and (*c*) the connectivity of the BTC ligand in UOW-10.

al., 2015). Sodium cations are located between the 2D layers, while the cobalt and molybdenum cations are approximately in the plane of the BTC linkers.

As seen in Fig. S4, comparing the IR spectra of UOW-10 and $Na_2MoO_4{\cdot}2H_2O$ in the range 1000–825 cm^{-1}, the region corresponding to Mo═O and Mo—O stretches, shows close agreement, thereby providing further evidence of the MoO_4 tetrahedral units in the structure. The Mo—O bond lengths vary between 1.699 (10) and 1.731 (7) Å, which is similar to what is seen in other molybdates (Chithambararaj *et al.*, 2013). Bond valence sums (Table S4) indicate that the oxidation state of molybdenum is Mo^{VI} (Chen *et al.*, 2002).

One of the more interesting features of the structure of UOW-10 is the presence of a five-coordinate Co^{2+} metal centre. In UOW-10, the trigonal bipyramidal coordination geometry of the cobalt is achieved as a consequence of edge-sharing O atoms with two sodium sites, as well as corner-sharing with a third sodium and one molybdenum site. This coordination environment would prevent the coordination of, for example, additional solvent molecules which would otherwise allow the system to achieve octahedral geometry. Although rare, trigonal bipyramidal geometries have been observed in molecular complexes. These cases typically involve the use of bulky chelating ligands to stabilize the geometry. Among inorganic materials, the five-coordinate CoO_5 configuration is relatively rare, with only 138 crystal structures reported in the ICSD, compared to 1624 for CoO_6 and 232 for CoO_4. This trend is consistent with the CSD where there are 4397 CoO_6 structures, 551 CoO_4 structures and 360 CoO_5 structures. Among the CoO_5-containing compounds many incorporate tetrahedral structural units – including molybdates, sulfates, phosphates, vanadates and arsenates (Engel *et al.*, 2009; Lü *et al.*, 2014; Baies *et al.*, 2006; Smith Pellizzeri *et al.*, 2020; de Pedro *et al.*, 2010). This could indicate that tetrahedral structural units can help stabilize lower cobalt coordination geometries, as seen in UOW-10.

Usually, cobalt-containing MOFs contain the metal in sites that are either four- or six-coordinate. For example, in cobalt-based zeolitic imidazolate frameworks (ZIFs), the cobalt cation is typically coordinated by four imidazolate ligands to afford tetrahedrally coordinated metal centres (Park *et al.*, 2006). In contrast, in cobalt-based Hofmann clathrates, cobalt is six-coordinate, with four cyano groups coordinating in equatorial positions and nitrogen-containing ligands in axial positions (Pei *et al.*, 2022). Notably, cobalt MOFs can reversibly transform between six- and four-coordinate structures; for example, in PCN-224(Co), where the cobalt metal centres in the porphyrin core are six-coordinate (four equatorial N atoms and two axial solvent molecules), upon activation the solvent molecules can be removed and the coordination number reduced to four to yield a square-planar Co^{II} metal centre.

Cobalt-based MOFs can also reversibly transform from six- to five-coordinate structures to generate square-pyramidal coordination geometry. This is more commonly seen in triazolate-based MOFs such as MAF-X27, MIT-20 and Co-BTTri (Liao *et al.*, 2015; Park *et al.*, 2017; Xiao *et al.*, 2016). There are some carboxylate-based systems which can also generate this coordination geometry. For example, MOF-74(Co) (also known as CPO-27) (Rosi *et al.*, 2005; Dietzel *et al.*, 2008) and its isorecticular analogues (Peng *et al.*, 2020; Ahmed *et al.*, 2024) once dehydrated show a square-pyramidal coordination geometry. Cobalt MOFs with trigonal bipyramidal coordination geometries have been reported previously, usually appearing in mixed-ligand systems that contain both carboxylate and nitrogen-based donors (Geng *et al.*, 2012). In cases where this coordination geometry is solely observed with carboxylate-based donors, the inorganic building unit is usually a chain or cluster as opposed to a monometallic metal node (Kim *et al.*, 2012; Wang *et al.*, 2013; Sarma *et al.*, 2012).

In order to verify the structural model from the 3D ED and to verify the purity of the bulk sample, high-resolution synchrotron PXRD data were collected. As seen in Fig. 4, the Rietveld fit (R_{wp} = 4.92%) confirms that the structural model is representative of the bulk material and the sample is of high purity since no other diffraction peaks are observed. The

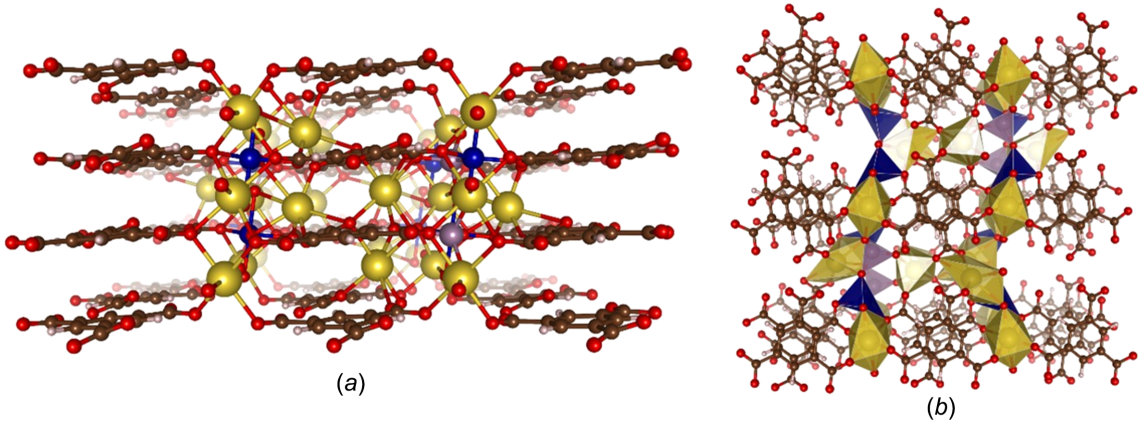

Figure 3
Extended views of UOW-10, with Co atoms shown in dark blue, Na atoms shown in yellow, Mo shown in purple and O, C and H atoms shown in red, brown and white, respectively. (*a*) View of the structure along the crystallographic *b* axis, revealing the sodium columns separated by Co and Mo atoms. (*b*) View of the structure along the crystallographic *c* axis. Na, Co and Mo polyhedra are shown in gold, blue and purple, respectively.

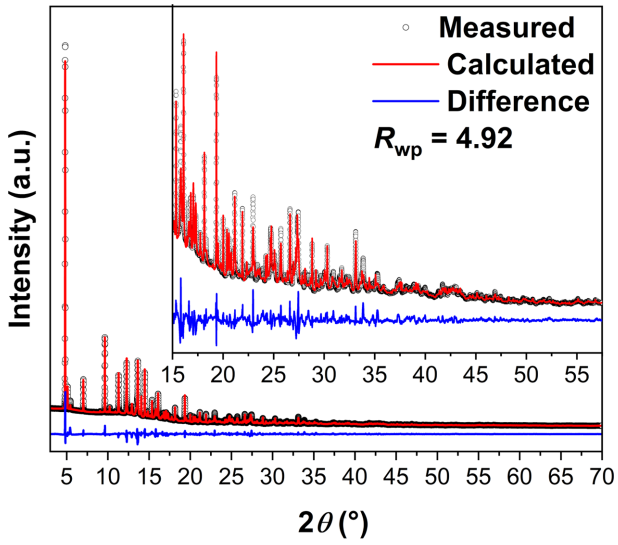

Figure 4
Final Rietveld fit for UOW-10 using the 3D ED structure against synchrotron powder X-ray diffraction data [λ = 0.8249705 (3) Å]. See text for refined lattice parameters.

refined lattice parameters [a = 9.88678 (11), b = 18.53948 (15), c = 6.99808 (9) Å, $\alpha = \gamma = 90$ and β = 96.382 (5)°] are in good agreement with those obtained from 3D ED [a = 9.718 (2), b = 18.250 (3), c = 6.892 (9) Å, $\alpha = \gamma = 90$ and β = 96.156 (15)°].

3.2. Optical properties

The UV–Vis diffuse reflectance spectrum [Fig. 5(*a*)] shows the existence of two main features, one centred in the UV region and the other in the visible-light region. The first feature appears in the range 200–300 nm and is very similar to that seen in the acid form of the ligand, H_3BTC, with a slight red shift. This feature most likely corresponds to π–π^* transitions within the BTC ligand, in good agreement with what has been observed previously in the literature for other BTC-based MOFs (Wang *et al.*, 2015). The feature seen in the visible-light region in the range 450–650 nm is more structured. Deconvolution of this region reveals that four peaks make up the signal [Fig. 5(*b*) and Table S5]. Interestingly, the UV–Vis spectrum of UOW-10 shares similarities with that of a mixed-ligand cobalt MOF, $[Co(C_{12}H_8N_2)(HO_3P–C_2H_4–PO_3H)]$, reported by Fu *et al.* (2007). This is presumably a consequence of cobalt also being in a trigonal bipyramidal coordination geometry in this structure. In their work, several transitions can be seen in the visible-light region at λ_{max} = 504, 534 and 624 nm. In UOW-10, four transitions can be seen in a similar region, *i.e.* λ_{max} = 506, 540, 575 and 623 nm. The transitions at 506, 575 and 623 nm can be attributed to *d*–*d* transitions from a trigonal bipyramidal crystal field of the cobalt metal centre (Companion & Komarynsky, 1964). Presumably the weak transition observed at 540 nm, which cannot be accounted for by crystal field splitting, is a spin-forbidden or vibronically allowed *d*–*d* transition. The corresponding Tauc plot [Fig. 5(*a*), inset] indicates that the material shows a bandgap of ∼1.8 eV.

3.3. Thermal stability of UOW-10

In order to gain insight into the thermal stability of UOW-10, a combination of variable-temperature *in-situ* PXRD (VT-PXRD) and thermogravimetric analysis (TGA) were used. As seen in Fig. 6(*a*), an initial small loss in mass (<3%) is observed in the range 35–410 °C. As there are no solvent molecules present in the crystal structure, this suggests this mass loss corresponds to the removal of surface solvent molecules. This is corroborated by VT-PXRD [Fig. 6(*b*)], which revealed that in this temperature range, crystallinity is maintained and the diffraction intensity remains constant. The VT-PXRD reveals

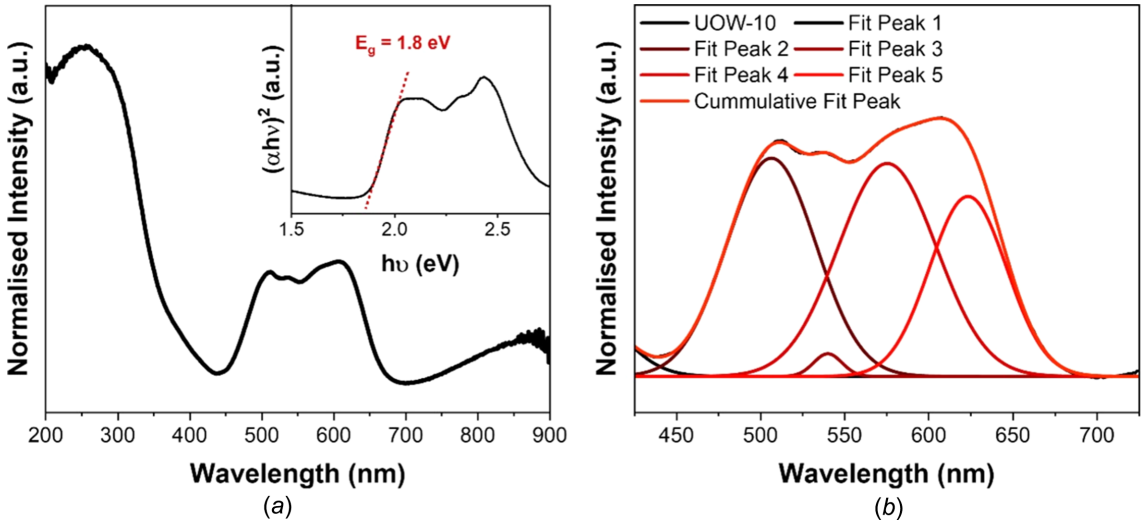

Figure 5
Optical properties of UOW-10. (*a*) UV–Vis diffuse reflectance spectrum of UOW-10 demonstrating that the sample absorbs in the UV and visible regions. The inset is a Tauc plot constructed from the UV–Vis data, indicating the existence of a band gap at 1.8 eV. (*b*) Deconvolution of the visible-light region of the UV–Vis spectrum.

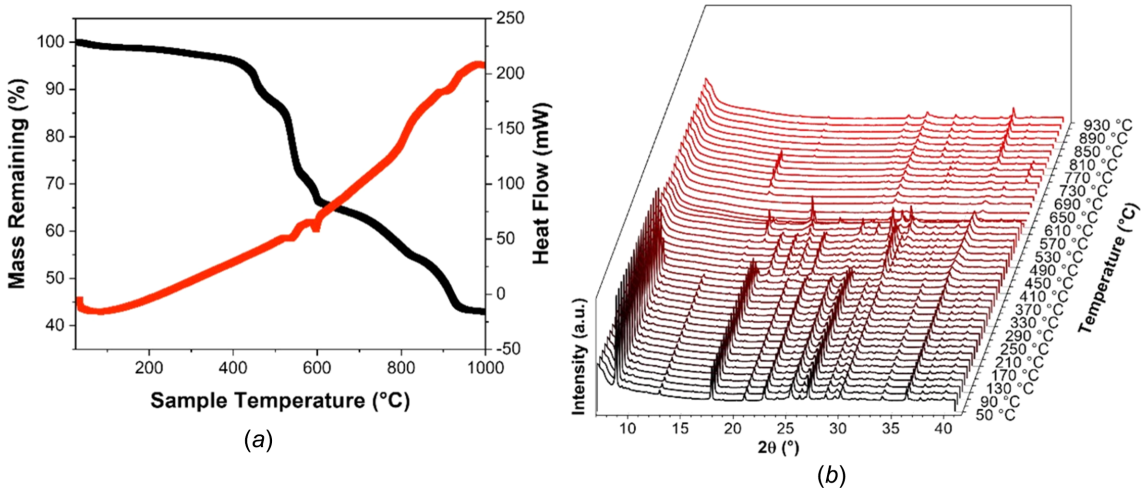

Figure 6
Assessing the thermal stability of UOW-10. (*a*) Thermogravimetric analysis (TGA) data collected from 50 to 1000 °C and (*b*) variable-temperature powder X-ray diffraction (VT-PXRD) of UOW-10 demonstrating the good thermal stability of the material and the formation of several phases upon structure collapse at temperatures greater than 410 °C.

that above 410 °C the framework begins to collapse as Bragg peaks associated with UOW-10 begin to decrease in intensity, while new peaks associated with another phase begin to increase in intensity. This result is corroborated by the TGA which shows the onset of a significant mass loss. Between 430 and 920 °C, PXRD shows several distinct changes which implies that several intermediate crystalline phases form in the decomposition process. This is also observed in the TGA, where there are several mass-loss features. Although the identity of the intermediate phases could not be identified, the Bragg peaks observed appear at higher angles than initially present in UOW-10, indicating that the intermediate materials have smaller unit cells, and likely correspond to dense phases. After heating at 930 °C, the remaining material can be assigned as being a mixture that contains Na_2MoO_4, CoO and Co_3Mo (Fig. S5).

4. Conclusion

A novel trimetallic cobalt-, molybdenum- and sodium-containing metal–organic framework constructed using a commercially available organic ligand, benzene-1,3,5-tricarboxylate, was crystallized directly under hydrothermal conditions. The material presents a unique structure which unusually contains five-coordinate Co^{2+} connected to both Na and Mo *via* shared O atoms. Although this leads to a rather dense structure, the characterization of this phase suggests that other heterometallic MOFs may be possible with unique structures, if more extended linkers were to be used.

Acknowledgements

The research benefited from the equipment made available by the University of Warwick Research Technology Platforms, and we thank the EPSRC for funding (EP/X014606/1, A National Electron Diffraction Facility for Nanomaterial Structural Studies). We thank Diamond Light Source for beamtime at I11 (Block Allocation Grant CY25166).

Conflict of interest

There are no conflicts to report.

Funding information

Funding for this research was provided by: Engineering and Physical Sciences Research Council (grant No. EP/X014606/1 to Richard I. Walton).

References

Ahmed, A., Kelly, A., Leonard, D., Saleem, W., Bezrukov, A., Efthymiou, C. G., Zaworotko, M. J., Tiana, D., Boyd, A. & Papatriantafyllopoulou, C. (2024). *Dalton Trans.* **53**, 11867–11875.
Allen, F. H. & Bruno, I. J. (2010). *Acta Cryst.* B**66**, 380–386.
Baies, R., Pérez, O., Caignaert, V., Pralong, V. & Raveau, B. (2006). *J. Mater. Chem.* **16**, 2434–2438.
Batten, S. R., Champness, N. R., Chen, X.-M., Garcia-Martinez, J., Kitagawa, S., Öhrström, L., O'Keeffe, M., Suh, M. P. & Reedijk, J. (2012). *CrystEngComm* **14**, 3001.
Bourhis, L. J., Dolomanov, O. V., Gildea, R. J., Howard, J. A. K. & Puschmann, H. (2015). *Acta Cryst.* A**71**, 59–75.
Brown, I. D. & Altermatt, D. (1985). *Acta Cryst.* B**41**, 244–247.
Castells-Gil, J. M., Padial, N., Almora-Barrios, N., Gil-San-Millán, R., Romero-Ángel, M., Torres, V., da Silva, I., Vieira, B. C. J., Waerenborgh, J. C., Jagiello, J., Navarro, J. A. R., Tatay, S. & Martí-Gastaldo, C. (2020). *Chem* **6**, 3118–3131.
Chambers, M. B., Wang, X., Ellezam, L., Ersen, O., Fontecave, M., Sanchez, C., Rozes, L. & Mellot-Draznieks, C. (2017). *J. Am. Chem. Soc.* **139**, 8222–8228.
Chen, J., An, B., Chen, Y., Han, X., Mei, Q., He, M., Cheng, Y., Vitorica-Yrezabal, I. J., Natrajan, L. S., Lee, D., Ramirez-Cuesta, A. J., Yang, S. & Schröder, M. (2023). *J. Am. Chem. Soc.* **145**, 19225–19231.
Chen, M., Zhou, Z. & Hu, S. (2002). *Chin. Sci. Bull.* **47**, 978–981.

Chithambararaj, A., Sanjini, N. S., Bose, A. C. & Velmathi, S. (2013). *Catal. Sci. Technol.* **3**, 1405.
Coelho, A. A. (2018). *J. Appl. Cryst.* **51**, 210–218.
Companion, A. L. & Komarynsky, M. A. (1964). *J. Chem. Educ.* **41**, 257.
de Pedro, I., Rojo, J. M., Rodríguez Fernández, J., Fernández-Díaz, M. T. & Rojo, T. (2010). *Phys. Rev. B* **81**, 134431.
Dhakshinamoorthy, A., Li, Z. & Garcia, H. (2018). *Chem. Soc. Rev.* **47**, 8134–8172.
Dietzel, P. D. C., Johnsen, R. E., Blom, R. & Fjellvåg, H. (2008). *Chem. Eur. J.* **14**, 2389–2397.
Dolomanov, O. V., Bourhis, L. J., Gildea, R. J., Howard, J. A. K. & Puschmann, H. (2009). *J. Appl. Cryst.* **42**, 339–341.
Engel, J. M., Ahsbahs, H., Fuess, H. & Ehrenberg, H. (2009). *Acta Cryst.* B**65**, 29–35.
Farrusseng, D., Aguado, S. & Pinel, C. (2009). *Angew. Chem. Int. Ed.* **48**, 7502–7513.
Fu, S.-J., Cheng, C.-Y. & Lin, K.-J. (2007). *Cryst. Growth Des.* **7**, 1381–1384.
Geng, J. C., Liu, L. W., Xiao, S. L. & Cui, G. H. (2012). *Transition Met. Chem.* **38**, 143–148.
Groom, C. R., Bruno, I. J., Lightfoot, M. P. & Ward, S. C. (2016). *Acta Cryst.* B**72**, 171–179.
Han, X., Yang, S. & Schröder, M. (2019). *Nat. Rev. Chem.* **3**, 108–118.
Hao, J., Xu, X., Fei, H., Li, L. & Yan, B. (2018). *Adv. Mater.* **30**, 1705634.
Helal, A., Yamani, Z. H., Cordova, K. E. & Yaghi, O. M. (2017). *Natl Sci. Rev.* **4**, 296–298.
Kim, D., Song, X., Yoon, J. H. & Lah, M. S. (2012). *Cryst. Growth Des.* **12**, 4186–4193.
Kim, E. J., Siegelman, R. L., Jiang, H. Z., Forse, A. C., Lee, J.-H., Martell, J. D., Milner, P. J., Falkowski, J. M., Neaton, J. B., Reimer, J. A., Weston, S. C. & Long, J. R. (2020). *Science* **369**, 392–396.
Koo, W.-T., Jang, J.-S. & Kim, I.-D. (2019). *Chem* **5**, 1938–1963.
Lawson, H. D., Walton, S. P. & Chan, C. (2021). *Appl. Mater. Interfaces* **13**, 7004–7020.
Li, J.-R., Kuppler, R. J. & Zhou, H.-C. (2009). *Chem. Soc. Rev.* **38**, 1477–1504.
Liao, P.-Q., Chen, H., Zhou, D.-D., Liu, S.-Y., He, C.-T., Rui, Z., Ji, H., Zhang, J.-P. & Chen, X.-M. (2015). *Energy Environ. Sci.* **8**, 1011–1016.
Lü, M., Colmont, M., Kabbour, H., Colis, S. & Mentré, O. (2014). *Inorg. Chem.* **53**, 6969–6978.
Maiti, S., Pramanik, A., Manju, U. & Mahanty, S. (2015). *Appl. Mater. Interfaces* **7**, 16357–16363.
Maza, W. A., Padilla, R. & Morris, A. J. (2015). *J. Am. Chem. Soc.* **137**, 8161–8168.
Park, K. S., Ni, Z., Côté, A. P., Choi, J. Y., Huang, R., Uribe-Romo, F. J., Chae, H. K., O'Keeffe, M. & Yaghi, O. M. (2006). *PNAS* **103**, 10186–10191.
Park, S. S., Tulchinsky, Y. & Dincă, M. (2017). *J. Am. Chem. Soc.* **139**, 13260–13263.
Pei, J., Gu, X.-W., Liang, C.-C., Chen, B., Li, B. & Qian, G. (2022). *J. Am. Chem. Soc.* **144**, 3200–3209.
Peng, S., Bie, B., Jia, H., Tang, H., Zhang, X., Sun, Y., Wei, Q., Wu, F., Yuan, Y., Deng, H. & Zhou, X. (2020). *J. Am. Chem. Soc.* **142**, 5049–5059.
Rigaku OD (2025). *CrysAlis PRO*. Rigaku Oxford Diffraction Ltd, Yarnton, Oxfordshire, England.
Rosi, N. L., Kim, J., Eddaoudi, M., Chen, B., O'Keeffe, M. & Yaghi, O. M. (2005). *J. Am. Chem. Soc.* **127**, 1504–1518.
Saha, A., Nia, S. S. & Rodríguez, J. A. (2022). *Chem. Rev.* **122**, 13883–13914.
Sarma, D., Mahata, P., Natarajan, S., Panissod, P., Rogez, G. & Drillon, M. (2012). *Inorg. Chem.* **51**, 4495–4501.
Sharma, A., Lim, J. & Lah, M. S. (2023). *Coord. Chem. Rev.* **479**, 214995.
Sheldrick, G. M. (2015). *Acta Cryst.* A**71**, 3–8.
Smith Pellizzeri, T. M., Sanjeewa, L. D., Pellizzeri, S., McMillen, C. D., Garlea, V. O., Ye, F., Sefat, A. S. & Kolis, J. W. (2020). *Dalton Trans.* **49**, 4323–4335.
Sun, D., Fu, Y., Liu, W., Ye, L., Wang, D., Yang, L., Fu, X. & Li, Z. (2013). *Chem. A Eur. J.* **19**, 14279–14285.
Wang, G., Liu, Y., Huang, B., Qin, X., Zhang, X. & Dai, Y. (2015). *Dalton Trans.* **44**, 16238–16241.
Wang, L. J., Deng, H., Furukawa, H., Gándara, F., Cordova, K. E., Peri, D. & Yaghi, O. M. (2014). *Inorg. Chem.* **53**, 5881–5883.
Wang, X., Huang, J., Liu, L., Liu, G., Lin, H., Zhang, J., Chen, N. & Qu, Y. (2013). *RSC Adv.* **3**, 13944.
Wei, Y.-S., Zhang, M., Zou, R. & Xu, Q. (2020). *Chem. Rev.* **120**, 12089–12174.
Xiao, D. J., Gonzalez, M. I., Darago, L. E., Vogiatzis, K. D., Haldoupis, E., Gagliardi, L. & Long, J. R. (2016). *J. Am. Chem. Soc.* **138**, 7161–7170.
Xiao, Y., Bu, X. & Feng, P. (2025). *Angew. Chem. Int. Ed.* **64**, e202422635.
Yuan, S., Chen, Y.-P., Qin, J.-S., Lu, W., Zou, L., Zhang, Q., Wang, X., Sun, X. & Zhou, H.-C. (2016). *J. Am. Chem. Soc.* **138**, 8912–8919.
Yuan, S., Lu, W., Chen, Y.-P., Zhang, Q., Liu, T.-F., Feng, D., Wang, X., Qin, J. & Zhou, H.-C. (2015). *J. Am. Chem. Soc.* **137**, 3177–3180.
Yuan, S., Qin, J.-S., Xu, H.-Q., Su, J., Rossi, D., Chen, Y., Zhang, L., Lollar, C., Wang, Q., Jiang, H.-L., Son, D. H., Xu, H., Huang, Z., Zou, X. & Zhou, H.-C. (2017). *ACS Cent. Sci.* **4**, 105–111.

supporting information

Acta Cryst. (2026). C**82**, 102-109 [https://doi.org/10.1107/S205322962600077X]

Structure and optical properties of a trimetallic cobalt–molybdenum–sodium metal–organic framework

Benjamin J. Moore, Jeremiah P. Tidey, Craig I. Hiley and Richard I. Walton

Computing details

Poly[μ-benzene-1,3,5-tricarboxylato-tetra-μ-oxido-cobaltmolybdenumtrisodium]

Crystal data

$[Na_3Co(MoO_4)(C_9H_3O_6)]$
M_r = 494.96
Monoclinic, $P2_1/c$
a = 9.718 (2) Å
b = 18.250 (3) Å
c = 6.8892 (9) Å
β = 96.156 (15)°
V = 1214.7 (4) Å^3
Z = 4
$F(000)$ = 301.632
D_x = 2.707 Mg m^{-3}
Electron radiation, λ = 0.0251 Å
Cell parameters from 1788 reflections
θ = 0.1–0.9°
μ = Not calculated mm^{-1}
T = 293 K
Microcrystalline slabs, bulk purple

Data collection

XtaLAB Synergy-ED, HyPix-ED, electron source at 200keV diffractometer
Radiation source: electron diffractometer, JEOL JEM-2300ED, LaB_6
None monochromator
Detector resolution: 10.0000 pixels mm^{-1}
continuous rotation electron diffraction scans
3862 measured reflections
3862 independent reflections
3183 reflections with $I \geq 2u(I)$
R_{int} = 0.181
θ_{max} = 0.9°, θ_{min} = 0.1°
h = −12→11
k = −22→22
l = −8→8

Refinement

Refinement on F^2
Least-squares matrix: full
$R[F^2 > 2\sigma(F^2)]$ = 0.182
$wR(F^2)$ = 0.406
S = 1.04
3862 reflections
222 parameters
108 restraints
6 constraints
Primary atom site location: dual
Secondary atom site location: difference Fourier map
H-atom parameters constrained
$w = 1/[\sigma^2(F_o^2) + (0.1111P)^2 + 3.0797P]$ where $P = (F_o^2 + 2F_c^2)/3$
$(\Delta/\sigma)_{max}$ = −0.001
$\Delta\rho_{max}$ = 1.67 e Å^{-3}
$\Delta\rho_{min}$ = −1.54 e Å^{-3}

Special details

Refinement. An extinction correction was refined to broadly account for the impact of multiple diffraction on the data in the kinematic approximation.
Global rigid bond (RIGU) restraints were employed to eliminate non-positive definite ADPs and improve their physical shape, alongside select isotropicity (ISOR) and proximal similarity (SIMU) restraints.
C-H H-atoms are placed geometrically at neutron standard distances with riding isotropic displacement parameters.
56 reflections were omitted as outliers in the final stages of refinement for which Fo particularly deviated from the general trend and spread, testing these with refinement and concluding them to be more significantly affected by multiple diffraction and of no merit to the refinement.

Fractional atomic coordinates and isotropic or equivalent isotropic displacement parameters (Å²)

	x	*y*	*z*	U_{iso}*/U_{eq}
Mo1	0.9853 (2)	0.82601 (10)	0.7514 (3)	0.0127 (7)
Co1	1.0350 (3)	0.63269 (13)	0.7610 (4)	0.0112 (8)
O4	1.0301 (9)	0.8755 (4)	0.5578 (11)	0.0170 (18)
Na1	0.6696 (8)	0.7450 (4)	0.9619 (10)	0.0247 (17)
Na4	0.2664 (10)	0.7242 (5)	0.5764 (11)	0.037 (2)
Na3	1.0	1.0	0.5	0.025 (2)
O6	0.8767 (8)	0.5615 (4)	0.7286 (11)	0.0145 (16)
Na2	1.0	0.5	0.5	0.022 (2)
O3	1.0611 (8)	0.7401 (3)	0.7598 (11)	0.0134 (16)
O9	0.1590 (10)	0.5164 (5)	0.7718 (13)	0.029 (2)
O2	0.8110 (10)	0.8137 (5)	0.7317 (15)	0.033 (2)
C8	0.5671 (10)	0.3389 (5)	0.7646 (14)	0.017 (2)
O8	0.4831 (11)	0.2995 (4)	0.8243 (17)	0.042 (3)
C3	0.5495 (10)	0.4198 (5)	0.7613 (14)	0.020 (2)
O7	0.6762 (10)	0.3155 (4)	0.7060 (14)	0.032 (2)
O10	0.2516 (10)	0.6234 (4)	0.7858 (14)	0.030 (2)
C1	0.6402 (10)	0.5403 (4)	0.7374 (14)	0.0182 (19)
C7	0.7572 (10)	0.5911 (4)	0.7268 (15)	0.022 (2)
C2	0.6562 (11)	0.4650 (5)	0.7378 (14)	0.023 (2)
H2	0.7562 (11)	0.4420 (5)	0.7189 (14)	0.034 (3)*
C4	0.4181 (11)	0.4494 (5)	0.7752 (15)	0.025 (2)
H4	0.3314 (11)	0.4134 (5)	0.7884 (15)	0.038 (3)*
O5	0.7439 (9)	0.6556 (4)	0.7277 (13)	0.026 (2)
C5	0.3991 (11)	0.5227 (5)	0.7723 (15)	0.022 (2)
C6	0.5071 (11)	0.5693 (5)	0.7502 (15)	0.023 (2)
H6	0.4901 (11)	0.6277 (5)	0.7426 (15)	0.035 (3)*
C9	0.2588 (10)	0.5560 (5)	0.7760 (13)	0.016 (2)
O1	1.0376 (9)	0.8744 (4)	0.9585 (10)	0.0184 (19)

Atomic displacement parameters (Å²)

	U^{11}	U^{22}	U^{33}	U^{12}	U^{13}	U^{23}
Mo1	0.0165 (14)	0.0108 (10)	0.0109 (10)	0.0017 (8)	0.0023 (8)	−0.0020 (8)
Co1	0.0142 (18)	0.0091 (13)	0.0116 (14)	−0.0020 (10)	0.0070 (12)	0.0030 (11)
O4	0.023 (5)	0.014 (3)	0.017 (3)	0.010 (2)	0.011 (2)	0.0021 (16)
Na1	0.022 (5)	0.027 (4)	0.027 (4)	0.003 (3)	0.009 (3)	0.006 (3)

Na4	0.044 (6)	0.045 (5)	0.026 (4)	−0.017 (4)	0.023 (4)	−0.009 (4)
Na3	0.030 (7)	0.013 (3)	0.033 (5)	0.005 (3)	0.012 (4)	0.003 (2)
O6	0.007 (4)	0.018 (4)	0.018 (4)	0.000 (3)	0.002 (3)	0.001 (3)
Na2	0.017 (6)	0.012 (5)	0.039 (6)	−0.006 (4)	0.006 (4)	−0.004 (4)
O3	0.016 (3)	0.006 (3)	0.020 (3)	−0.0025 (17)	0.0068 (18)	−0.0018 (18)
O9	0.018 (6)	0.043 (5)	0.029 (5)	−0.011 (4)	0.013 (4)	−0.001 (4)
O2	0.023 (6)	0.025 (4)	0.052 (6)	−0.002 (4)	0.003 (4)	−0.012 (4)
C8	0.012 (5)	0.011 (4)	0.029 (4)	0.003 (3)	0.014 (3)	0.004 (3)
O8	0.044 (7)	0.009 (4)	0.082 (7)	−0.002 (3)	0.042 (5)	0.003 (4)
C3	0.013 (5)	0.011 (4)	0.038 (4)	0.003 (3)	0.011 (3)	0.005 (3)
O7	0.026 (6)	0.019 (4)	0.052 (6)	−0.003 (3)	0.009 (5)	−0.010 (4)
O10	0.038 (7)	0.018 (4)	0.038 (5)	0.008 (4)	0.017 (4)	0.011 (4)
C1	0.007 (4)	0.010 (3)	0.038 (4)	0.000 (2)	0.005 (2)	0.002 (2)
C7	0.013 (6)	0.008 (4)	0.045 (5)	0.001 (3)	0.008 (4)	−0.002 (3)
C2	0.011 (5)	0.017 (4)	0.042 (5)	0.003 (3)	0.005 (3)	0.007 (3)
C4	0.015 (5)	0.015 (4)	0.047 (5)	0.001 (3)	0.010 (3)	0.001 (3)
O5	0.009 (4)	0.027 (4)	0.044 (4)	−0.003 (2)	0.008 (3)	−0.001 (3)
C5	0.011 (5)	0.013 (4)	0.042 (4)	0.002 (2)	0.004 (3)	−0.001 (3)
C6	0.012 (5)	0.009 (4)	0.049 (5)	0.002 (3)	0.008 (3)	0.005 (3)
C9	0.011 (4)	0.016 (3)	0.020 (3)	0.0023 (18)	0.0017 (18)	−0.0010 (18)
O1	0.031 (6)	0.012 (4)	0.014 (4)	0.003 (3)	0.013 (3)	0.005 (3)

Geometric parameters (Å, º)

Mo1—O4	1.705 (7)	Na4—O7^{xi}	2.203 (12)
Mo1—Na1^{i}	3.709 (8)	Na4—O10	2.353 (11)
Mo1—Na4^{ii}	3.465 (9)	Na4—O1^{x}	2.909 (12)
Mo1—Na4^{iii}	3.616 (9)	Na3—O6^{xii}	2.390 (7)
Mo1—Na3^{iv}	3.6269 (19)	Na3—O6^{i}	2.390 (7)
Mo1—Na2^{v}	3.6034 (19)	Na3—Na2^{xii}	3.4446
Mo1—O3	1.731 (7)	Na3—Na2^{xiii}	3.4446
Mo1—O2	1.699 (10)	Na3—O9^{xiv}	2.339 (9)
Mo1—O1	1.709 (8)	Na3—O9^{vii}	2.339 (9)
Co1—O4^{v}	2.056 (7)	O6—Na2	2.362 (7)
Co1—Na4^{iii}	3.175 (8)	O6—C7	1.280 (12)
Co1—Na3^{vi}	2.968 (3)	Na2—O9^{iii}	2.316 (9)
Co1—O6	2.008 (8)	Na2—O9^{xi}	2.316 (9)
Co1—Na2	3.013 (3)	Na2—O1^{vi}	2.343 (7)
Co1—O3	1.976 (7)	Na2—O1^{i}	2.343 (7)
Co1—O10^{iii}	2.100 (10)	O9—C9	1.207 (12)
Co1—O1^{i}	2.090 (7)	C8—O8	1.193 (12)
O4—Na3^{iv}	2.321 (7)	C8—C3	1.486 (12)
Na1—Na1^{i}	3.4494 (7)	C8—O7	1.250 (13)
Na1—Na1^{v}	3.4494	C3—C2	1.349 (13)
Na1—O2^{v}	2.438 (12)	C3—C4	1.399 (13)
Na1—O2	2.538 (12)	O10—C9	1.234 (11)
Na1—O8^{vii}	2.540 (14)	C1—C7	1.476 (13)
Na1—O8^{viii}	2.346 (12)	C1—C2	1.382 (11)

Na1—O5	2.457 (11)	C1—C6	1.409 (13)
Na1—O5^{v}	2.623 (11)	C7—O5	1.184 (11)
Na4—Na4^{i}	3.571 (4)	C2—H2	1.0800
Na4—Na4^{v}	3.571 (4)	C4—H4	1.0800
Na4—O3^{ix}	2.490 (11)	C4—C5	1.350 (12)
Na4—O3^{x}	2.869 (12)	C5—C6	1.372 (13)
Na4—C8^{vii}	2.796 (12)	C5—C9	1.496 (13)
Na4—O8^{vii}	2.815 (14)	C6—H6	1.0800
Na4—O7^{vii}	2.269 (12)		

Na1^{i}—Mo1—O4	91.8 (3)	O6^{xii}—Na3—Co1^{xii}	42.33 (18)
Na4^{iii}—Mo1—O4	75.3 (3)	O6^{i}—Na3—Co1^{xii}	137.67 (18)
Na4^{ii}—Mo1—O4	113.3 (3)	O6^{i}—Na3—Co1^{i}	42.33 (18)
Na4^{iii}—Mo1—Na1^{i}	104.62 (18)	O6^{xii}—Na3—Co1^{i}	137.67 (18)
Na4^{ii}—Mo1—Na1^{i}	143.55 (19)	O6^{xii}—Na3—O4^{iv}	73.6 (3)
Na3^{iv}—Mo1—O4	30.3 (2)	O6^{i}—Na3—O4	73.6 (3)
Na3^{iv}—Mo1—Na1^{i}	97.01 (13)	O6^{xii}—Na3—O4	106.4 (3)
Na3^{iv}—Mo1—Na4^{iii}	102.75 (13)	O6^{i}—Na3—O4^{iv}	106.4 (3)
Na3^{iv}—Mo1—Na4^{ii}	118.12 (16)	O6^{i}—Na3—O6^{xii}	180.0
Na2^{v}—Mo1—O4	84.5 (2)	Na2^{xiii}—Na3—Mo1^{iv}	61.21 (3)
Na2^{v}—Mo1—Na1^{i}	123.50 (13)	Na2^{xii}—Na3—Mo1	61.21 (3)
Na2^{v}—Mo1—Na4^{iii}	128.18 (15)	Na2^{xiii}—Na3—Mo1	118.79 (3)
Na2^{v}—Mo1—Na4^{ii}	86.42 (14)	Na2^{xii}—Na3—Mo1^{iv}	118.79 (3)
Na2^{v}—Mo1—Na3^{iv}	56.90 (3)	Na2^{xiii}—Na3—Co1^{xii}	124.54 (5)
O3—Mo1—O4	111.2 (4)	Na2^{xiii}—Na3—Co1^{i}	55.46 (5)
O3—Mo1—Na1^{i}	91.5 (3)	Na2^{xii}—Na3—Co1^{i}	124.54 (5)
O3—Mo1—Na4^{iii}	38.0 (3)	Na2^{xii}—Na3—Co1^{xii}	55.46 (5)
O3—Mo1—Na4^{ii}	55.6 (3)	Na2^{xiii}—Na3—O4	99.10 (18)
O3—Mo1—Na3^{iv}	140.4 (3)	Na2^{xii}—Na3—O4	80.90 (18)
O3—Mo1—Na2^{v}	141.9 (3)	Na2^{xiii}—Na3—O4^{iv}	80.90 (18)
O2—Mo1—O4	110.1 (5)	Na2^{xii}—Na3—O4^{iv}	99.10 (18)
O2—Mo1—Na1^{i}	31.9 (3)	Na2^{xiii}—Na3—O6^{i}	43.22 (18)
O2—Mo1—Na4^{iii}	133.4 (3)	Na2^{xiii}—Na3—O6^{xii}	136.78 (18)
O2—Mo1—Na4^{ii}	136.6 (4)	Na2^{xii}—Na3—O6^{xii}	43.22 (18)
O2—Mo1—Na3^{iv}	99.7 (3)	Na2^{xii}—Na3—O6^{i}	136.78 (18)
O2—Mo1—Na2^{v}	98.2 (3)	Na2^{xii}—Na3—Na2^{xiii}	180.0
O2—Mo1—O3	107.4 (4)	O9^{xiv}—Na3—Mo1	105.8 (2)
O1—Mo1—O4	107.5 (4)	O9^{xiv}—Na3—Mo1^{iv}	74.2 (2)
O1—Mo1—Na1^{i}	141.7 (3)	O9^{vii}—Na3—Mo1	74.2 (2)
O1—Mo1—Na4^{iii}	112.1 (3)	O9^{vii}—Na3—Mo1^{iv}	105.8 (2)
O1—Mo1—Na4^{ii}	56.9 (3)	O9^{xiv}—Na3—Co1^{i}	53.1 (2)
O1—Mo1—Na3^{iv}	85.6 (2)	O9^{xiv}—Na3—Co1^{xii}	126.9 (2)
O1—Mo1—Na2^{v}	32.3 (2)	O9^{vii}—Na3—Co1^{i}	126.9 (2)
O1—Mo1—O3	110.7 (4)	O9^{vii}—Na3—Co1^{xii}	53.1 (2)
O1—Mo1—O2	109.8 (4)	O9^{xiv}—Na3—O4^{iv}	95.2 (3)
Na4^{iii}—Co1—O4^{v}	122.0 (3)	O9^{xiv}—Na3—O4	84.8 (3)
Na3^{vi}—Co1—O4^{v}	51.2 (2)	O9^{vii}—Na3—O4	95.2 (3)
Na3^{vi}—Co1—Na4^{iii}	141.2 (2)	O9^{vii}—Na3—O4^{iv}	84.8 (3)

O6—Co1—O4^{v}	88.0 (3)	O9^{vii}—Na3—O6^{i}	105.9 (3)
O6—Co1—Na4^{iii}	149.7 (3)	O9^{vii}—Na3—O6^{xii}	74.1 (3)
O6—Co1—Na3^{vi}	53.2 (2)	O9^{xiv}—Na3—O6^{i}	74.1 (3)
Na2—Co1—O4^{v}	121.5 (2)	O9^{xiv}—Na3—O6^{xii}	105.9 (3)
Na2—Co1—Na4^{iii}	102.91 (16)	O9^{vii}—Na3—Na2^{xiii}	138.0 (2)
Na2—Co1—Na3^{vi}	70.31 (5)	O9^{xiv}—Na3—Na2^{xiii}	42.0 (2)
Na2—Co1—O6	51.5 (2)	O9^{xiv}—Na3—Na2^{xii}	138.0 (2)
O3—Co1—O4^{v}	95.3 (3)	O9^{vii}—Na3—Na2^{xii}	42.0 (2)
O3—Co1—Na4^{iii}	51.7 (3)	O9^{xiv}—Na3—O9^{vii}	180.0
O3—Co1—Na3^{vi}	146.5 (3)	Na3^{vi}—O6—Co1	84.4 (3)
O3—Co1—O6	137.6 (3)	Na2—O6—Co1	86.8 (3)
O3—Co1—Na2	143.2 (3)	Na2—O6—Na3^{vi}	92.9 (3)
O10^{iii}—Co1—O4^{v}	92.4 (4)	C7—O6—Co1	114.2 (6)
O10^{iii}—Co1—Na4^{iii}	47.8 (3)	C7—O6—Na3^{vi}	125.8 (7)
O10^{iii}—Co1—Na3^{vi}	93.6 (2)	C7—O6—Na2	136.0 (7)
O10^{iii}—Co1—O6	134.9 (3)	Mo1^{vi}—Na2—Mo1^{i}	180.0
O10^{iii}—Co1—Na2	91.8 (3)	Co1^{xv}—Na2—Mo1^{i}	115.36 (6)
O10^{iii}—Co1—O3	87.3 (3)	Co1—Na2—Mo1^{vi}	115.36 (6)
O1^{i}—Co1—O4^{v}	172.3 (3)	Co1^{xv}—Na2—Mo1^{vi}	64.64 (6)
O1^{i}—Co1—Na4^{iii}	63.2 (3)	Co1—Na2—Mo1^{i}	64.64 (6)
O1^{i}—Co1—Na3^{vi}	121.1 (2)	Co1^{xv}—Na2—Co1	180.0
O1^{i}—Co1—O6	86.6 (3)	Na3^{vi}—Na2—Mo1^{i}	118.11 (3)
O1^{i}—Co1—Na2	50.8 (2)	Na3^{vi}—Na2—Mo1^{vi}	61.89 (3)
O1^{i}—Co1—O3	92.4 (3)	Na3^{xvi}—Na2—Mo1^{vi}	118.11 (3)
O1^{i}—Co1—O10^{iii}	87.6 (4)	Na3^{xvi}—Na2—Mo1^{i}	61.89 (3)
Co1^{i}—O4—Mo1	140.8 (4)	Na3^{vi}—Na2—Co1^{xv}	125.77 (5)
Na3^{iv}—O4—Mo1	127.9 (4)	Na3^{xvi}—Na2—Co1^{xv}	54.23 (5)
Na3^{iv}—O4—Co1^{i}	85.2 (3)	Na3^{xvi}—Na2—Co1	125.77 (5)
Na1^{v}—Na1—Mo1^{v}	64.54 (13)	Na3^{vi}—Na2—Co1	54.23 (5)
Na1^{i}—Na1—Mo1^{v}	117.82 (16)	Na3^{vi}—Na2—Na3^{xvi}	180.0
O2^{v}—Na1—Mo1^{v}	21.6 (2)	O6^{xv}—Na2—Mo1^{i}	95.66 (17)
O2—Na1—Mo1^{v}	92.1 (3)	O6^{xv}—Na2—Mo1^{vi}	84.34 (17)
O2^{v}—Na1—Na1^{i}	136.4 (3)	O6—Na2—Mo1^{vi}	95.66 (17)
O2—Na1—Na1^{i}	44.9 (3)	O6—Na2—Mo1^{i}	84.34 (17)
O8^{viii}—Na1—Mo1^{v}	94.8 (4)	O6^{xv}—Na2—Co1^{xv}	41.72 (18)
O8^{vii}—Na1—Mo1^{v}	159.2 (3)	O6^{xv}—Na2—Co1	138.28 (18)
O8^{vii}—Na1—Na1^{i}	42.8 (3)	O6—Na2—Co1^{xv}	138.28 (18)
O8^{viii}—Na1—Na1^{i}	135.5 (4)	O6—Na2—Co1	41.72 (18)
O8^{viii}—Na1—O2	170.1 (5)	O6—Na2—Na3^{vi}	43.86 (17)
O8^{viii}—Na1—O2^{v}	73.2 (4)	O6^{xv}—Na2—Na3^{xvi}	43.86 (17)
O8^{vii}—Na1—O2^{v}	177.0 (5)	O6—Na2—Na3^{xvi}	136.14 (17)
O8^{vii}—Na1—O2	68.4 (3)	O6^{xv}—Na2—Na3^{vi}	136.14 (17)
O5^{v}—Na1—Mo1^{v}	73.5 (3)	O6^{xv}—Na2—O6	180.0
O5—Na1—Mo1^{v}	80.6 (3)	O9^{iii}—Na2—Mo1^{i}	105.0 (2)
O5—Na1—Na1^{i}	49.3 (3)	O9^{xi}—Na2—Mo1^{vi}	105.0 (2)
O5^{v}—Na1—Na1^{i}	129.1 (4)	O9^{iii}—Na2—Mo1^{vi}	75.0 (2)
O5—Na1—O2	72.6 (3)	O9^{xi}—Na2—Mo1^{i}	75.0 (2)
O5^{v}—Na1—O2	88.2 (4)	O9^{iii}—Na2—Co1	52.5 (2)

O5—Na1—O2^{v}	91.6 (4)	O9^{iii}—Na2—Co1^{xv}	127.5 (2)
O5^{v}—Na1—O2^{v}	71.4 (3)	O9^{xi}—Na2—Co1^{xv}	52.5 (2)
O5—Na1—O8^{vii}	86.5 (4)	O9^{xi}—Na2—Co1	127.5 (2)
O5^{v}—Na1—O8^{viii}	86.9 (4)	O9^{iii}—Na2—Na3^{xvi}	137.5 (2)
O5—Na1—O8^{viii}	115.6 (4)	O9^{xi}—Na2—Na3^{vi}	137.5 (2)
O5^{v}—Na1—O8^{vii}	111.4 (4)	O9^{iii}—Na2—Na3^{vi}	42.5 (2)
Co1^{ix}—Na4—Mo1^{ix}	62.85 (17)	O9^{xi}—Na2—Na3^{xvi}	42.5 (2)
Co1^{ix}—Na4—Mo1^{x}	64.93 (18)	O9^{iii}—Na2—O6^{xv}	104.9 (3)
Na4^{v}—Na4—Mo1^{x}	127.70 (14)	O9^{xi}—Na2—O6	104.9 (3)
Na4^{v}—Na4—Mo1^{ix}	57.65 (17)	O9^{iii}—Na2—O6	75.1 (3)
Na4^{i}—Na4—Mo1^{x}	61.83 (14)	O9^{xi}—Na2—O6^{xv}	75.1 (3)
Na4^{i}—Na4—Mo1^{ix}	105.3 (2)	O9^{xi}—Na2—O9^{iii}	180.0
Na4^{i}—Na4—Co1^{ix}	126.7 (2)	O1^{vi}—Na2—Mo1^{i}	157.09 (19)
Na4^{v}—Na4—Co1^{ix}	71.28 (18)	O1^{i}—Na2—Mo1^{i}	22.91 (19)
O3^{ix}—Na4—Mo1^{x}	74.9 (3)	O1^{vi}—Na2—Mo1^{vi}	22.91 (19)
O3^{x}—Na4—Mo1^{x}	29.87 (16)	O1^{i}—Na2—Mo1^{vi}	157.09 (19)
O3^{ix}—Na4—Mo1^{ix}	25.32 (19)	O1^{vi}—Na2—Co1	136.25 (18)
O3^{x}—Na4—Mo1^{ix}	69.4 (3)	O1^{vi}—Na2—Co1^{xv}	43.75 (18)
O3^{x}—Na4—Co1^{ix}	87.7 (3)	O1^{i}—Na2—Co1^{xv}	136.25 (18)
O3^{ix}—Na4—Co1^{ix}	38.50 (19)	O1^{i}—Na2—Co1	43.75 (18)
O3^{ix}—Na4—Na4^{i}	122.8 (3)	O1^{vi}—Na2—Na3^{vi}	82.03 (17)
O3^{x}—Na4—Na4^{i}	43.8 (2)	O1^{i}—Na2—Na3^{xvi}	82.03 (17)
C8^{vii}—Na4—Mo1^{x}	146.5 (4)	O1^{i}—Na2—Na3^{vi}	97.97 (17)
C8^{vii}—Na4—Mo1^{ix}	84.9 (3)	O1^{vi}—Na2—Na3^{xvi}	97.97 (17)
C8^{vii}—Na4—Co1^{ix}	129.9 (3)	O1^{vi}—Na2—O6	106.6 (2)
C8^{vii}—Na4—Na4^{i}	96.9 (3)	O1^{i}—Na2—O6	73.4 (2)
C8^{vii}—Na4—O3^{x}	117.0 (4)	O1^{i}—Na2—O6^{xv}	106.6 (2)
C8^{vii}—Na4—O3^{ix}	100.1 (4)	O1^{vi}—Na2—O6^{xv}	73.4 (2)
O8^{vii}—Na4—Mo1^{x}	152.6 (4)	O1^{vi}—Na2—O9^{iii}	97.3 (3)
O8^{vii}—Na4—Mo1^{ix}	109.4 (3)	O1^{vi}—Na2—O9^{xi}	82.7 (3)
O8^{vii}—Na4—Co1^{ix}	142.3 (4)	O1^{i}—Na2—O9^{iii}	82.7 (3)
O8^{vii}—Na4—Na4^{i}	90.9 (3)	O1^{i}—Na2—O9^{xi}	97.3 (3)
O8^{vii}—Na4—O3^{x}	125.9 (4)	O1^{i}—Na2—O1^{vi}	180.0
O8^{vii}—Na4—O3^{ix}	122.6 (4)	Co1—O3—Mo1	147.6 (5)
O8^{vii}—Na4—C8^{vii}	24.6 (3)	Na4^{iii}—O3—Mo1	116.7 (4)
O7^{vii}—Na4—Mo1^{ix}	62.9 (3)	Na4^{ii}—O3—Mo1	94.5 (3)
O7^{xi}—Na4—Mo1^{x}	66.4 (3)	Na4^{iii}—O3—Co1	89.8 (3)
O7^{xi}—Na4—Mo1^{ix}	137.3 (5)	Na4^{ii}—O3—Co1	107.5 (3)
O7^{vii}—Na4—Mo1^{x}	137.9 (5)	Na2^{ix}—O9—Na3^{xvii}	95.5 (3)
O7^{xi}—Na4—Co1^{ix}	116.0 (4)	C9—O9—Na3^{xvii}	130.3 (7)
O7^{vii}—Na4—Co1^{ix}	104.8 (3)	C9—O9—Na2^{ix}	124.2 (7)
O7^{xi}—Na4—Na4^{i}	37.7 (3)	Na1^{i}—O2—Mo1	126.5 (5)
O7^{vii}—Na4—Na4^{i}	114.7 (5)	Na1—O2—Mo1	128.1 (5)
O7^{vii}—Na4—O3^{ix}	74.5 (4)	O8—C8—Na4^{xvii}	78.6 (7)
O7^{xi}—Na4—O3^{ix}	141.1 (5)	C3—C8—Na4^{xvii}	144.2 (7)
O7^{xi}—Na4—O3^{x}	67.9 (4)	C3—C8—O8	121.4 (9)
O7^{vii}—Na4—O3^{x}	115.9 (4)	O7—C8—Na4^{xvii}	52.8 (6)
O7^{xi}—Na4—C8^{vii}	113.7 (4)	O7—C8—O8	122.7 (9)

O7^{vii}—Na4—C8^{vii}	26.0 (3)	O7—C8—C3	115.9 (8)
O7^{vii}—Na4—O8^{vii}	48.4 (3)	Na4^{xvii}—O8—Na1^{xvii}	114.5 (4)
O7^{xi}—Na4—O8^{vii}	94.7 (4)	Na4^{xvii}—O8—Na1^{viii}	105.5 (4)
O10—Na4—Mo1^{x}	95.4 (4)	C8—O8—Na1^{xvii}	109.4 (9)
O10—Na4—Mo1^{ix}	95.7 (3)	C8—O8—Na1^{viii}	158.0 (9)
O10—Na4—Co1^{ix}	41.4 (3)	C8—O8—Na4^{xvii}	76.9 (7)
O10—Na4—Na4^{i}	143.5 (5)	C2—C3—C8	121.4 (9)
O10—Na4—O3^{x}	124.1 (4)	C4—C3—C8	119.1 (8)
O10—Na4—O3^{ix}	71.0 (3)	C4—C3—C2	119.4 (8)
O10—Na4—C8^{vii}	114.6 (4)	C8—O7—Na4^{xvii}	101.2 (7)
O10—Na4—O8^{vii}	110.0 (5)	C8—O7—Na4^{xi}	134.5 (8)
O10—Na4—O7^{vii}	101.3 (4)	Na4—O10—Co1^{ix}	90.8 (4)
O10—Na4—O7^{xi}	108.8 (5)	C9—O10—Co1^{ix}	98.0 (7)
O1^{x}—Na4—Mo1^{x}	29.48 (17)	C9—O10—Na4	137.6 (8)
O1^{x}—Na4—Mo1^{ix}	80.1 (3)	C2—C1—C7	122.6 (8)
O1^{x}—Na4—Co1^{ix}	39.89 (18)	C6—C1—C7	119.0 (8)
O1^{x}—Na4—Na4^{i}	88.4 (2)	C6—C1—C2	118.5 (8)
O1^{x}—Na4—O3^{x}	58.6 (3)	C1—C7—O6	115.9 (7)
O1^{x}—Na4—O3^{ix}	65.4 (3)	O5—C7—O6	121.3 (9)
O1^{x}—Na4—C8^{vii}	164.9 (4)	O5—C7—C1	122.7 (9)
O1^{x}—Na4—O8^{vii}	170.2 (4)	C1—C2—C3	121.4 (9)
O1^{x}—Na4—O7^{xi}	78.9 (4)	H2—C2—C3	119.3 (6)
O1^{x}—Na4—O7^{vii}	139.9 (5)	H2—C2—C1	119.3 (6)
O1^{x}—Na4—O10	65.9 (3)	H4—C4—C3	119.8 (5)
Mo1—Na3—Mo1^{iv}	180.0	C5—C4—C3	120.4 (9)
Co1^{i}—Na3—Mo1	64.11 (6)	C5—C4—H4	119.8 (6)
Co1^{i}—Na3—Mo1^{iv}	115.89 (6)	C7—O5—Na1	134.7 (8)
Co1^{xii}—Na3—Mo1^{iv}	64.11 (6)	C7—O5—Na1^{i}	134.9 (8)
Co1^{xii}—Na3—Mo1	115.89 (6)	C6—C5—C4	120.8 (9)
Co1^{i}—Na3—Co1^{xii}	180.0	C9—C5—C4	121.7 (9)
O4—Na3—Mo1^{iv}	158.23 (18)	C9—C5—C6	117.3 (8)
O4^{iv}—Na3—Mo1^{iv}	21.77 (18)	C5—C6—C1	119.5 (8)
O4—Na3—Mo1	21.77 (18)	H6—C6—C1	120.3 (5)
O4^{iv}—Na3—Mo1	158.23 (18)	H6—C6—C5	120.3 (6)
O4—Na3—Co1^{xii}	136.35 (18)	O10—C9—O9	123.2 (10)
O4—Na3—Co1^{i}	43.65 (18)	C5—C9—O9	119.2 (9)
O4^{iv}—Na3—Co1^{i}	136.35 (18)	C5—C9—O10	117.6 (9)
O4^{iv}—Na3—Co1^{xii}	43.65 (18)	Co1^{v}—O1—Mo1	140.0 (4)
O4^{iv}—Na3—O4	180.0	Na4^{ii}—O1—Mo1	93.6 (3)
O6^{i}—Na3—Mo1	85.44 (17)	Na4^{ii}—O1—Co1^{v}	76.9 (3)
O6^{i}—Na3—Mo1^{iv}	94.56 (17)	Na2^{v}—O1—Mo1	124.8 (4)
O6^{xii}—Na3—Mo1	94.56 (17)	Na2^{v}—O1—Co1^{v}	85.4 (3)
O6^{xii}—Na3—Mo1^{iv}	85.44 (17)	Na2^{v}—O1—Na4^{ii}	134.1 (4)

Co1—O4^{v}—Mo1^{v}—Na1	40.9 (7)	Na4^{xvii}—C8—C3—C2	47.6 (12)
Co1^{i}—O4—Mo1—Na4^{iii}	63.8 (7)	Na4^{xvii}—C8—C3—C4	−134.9 (11)
Co1^{i}—O4—Mo1—Na4^{ii}	111.9 (7)	Na4^{xvii}—C8—O7—Na4^{xi}	126.1 (7)
Co1^{i}—O4—Mo1—Na3	−141.8 (12)	Na4^{xvii}—O8—C8—C3	−147.8 (6)

Co1^{i}—O4—Mo1—Na2^{v}	−164.4 (7)	Na4^{xvii}—O8—C8—O7	30.4 (8)
Co1^{i}—O4—Mo1—O3	51.4 (8)	Na4^{xi}—O7—C8—O8	87.6 (12)
Co1^{i}—O4—Mo1—O2	−67.6 (8)	Na4^{xvii}—O7—C8—O8	−38.5 (10)
Co1^{i}—O4—Mo1—O1	172.7 (7)	Na4^{xi}—O7—C8—C3	−94.2 (10)
Co1—O6—C7—C1	−169.9 (7)	Na4^{xvii}—O7—C8—C3	139.7 (6)
Co1—O6—C7—O5	6.0 (8)	Na4—O10—C9—O9	−105.6 (12)
Co1—O3—Mo1—O4	−122.2 (8)	Na4—O10—C9—C5	75.4 (12)
Co1—O3—Mo1—Na1^{i}	−29.7 (8)	Na4^{ii}—O1—Mo1—Na3	−128.0 (3)
Co1—O3—Mo1—Na4^{iii}	−141.9 (11)	Na4^{ii}—O1—Mo1—Na2^{v}	−153.3 (6)
Co1—O3—Mo1—Na4^{ii}	133.5 (9)	Na4^{ii}—O1—Mo1—O3	14.9 (4)
Co1—O3—Mo1—Na3	−132.6 (6)	Na4^{ii}—O1—Mo1—O2	133.4 (4)
Co1—O3—Mo1—Na2^{v}	128.5 (7)	Na3—Mo1—O1—Na2^{v}	25.38 (11)
Co1—O3—Mo1—O2	−1.6 (9)	Na3—O4—Mo1—Na2^{v}	−22.6 (5)
Co1—O3—Mo1—O1	118.3 (8)	Na3—O4—Mo1—O3	−166.8 (5)
Co1^{ix}—O10—C9—O9	−5.6 (8)	Na3—O4—Mo1—O2	74.2 (6)
Co1^{ix}—O10—C9—C5	175.4 (5)	Na3—O4—Mo1—O1	−45.5 (6)
Co1^{v}—O1—Mo1—O4	179.3 (7)	Na3^{v}—O6—C7—C1	−68.8 (7)
Co1^{v}—O1—Mo1—Na1^{i}	62.5 (9)	Na3^{vi}—O6—C7—C1	−68.8 (7)
Co1^{v}—O1—Mo1—Na4^{iii}	−99.9 (7)	Na3^{v}—O6—C7—O5	107.2 (8)
Co1^{v}—O1—Mo1—Na4^{ii}	−73.9 (7)	Na3^{vi}—O6—C7—O5	107.2 (8)
Co1^{v}—O1—Mo1—Na3	158.1 (7)	Na3^{xviii}—O9—C9—O10	−61.0 (11)
Co1—O1^{i}—Mo1^{i}—Na2	−132.8 (11)	Na3^{xvii}—O9—C9—O10	−61.0 (11)
Co1^{v}—O1—Mo1—O3	−59.0 (8)	Na3^{xvii}—O9—C9—C5	118.0 (9)
Co1^{v}—O1—Mo1—O2	59.5 (8)	Na3^{xviii}—O9—C9—C5	118.0 (9)
O4—Mo1—O3—Na4^{iii}	19.7 (4)	O6—C7—C1—C2	−3.6 (12)
O4—Mo1—O3—Na4^{ii}	104.4 (4)	O6—C7—C1—C6	175.5 (9)
O4—Mo1—O2—Na1	179.4 (4)	Na2^{xii}—Mo1—O4—Co1^{i}	−164.37 (14)
O4—Mo1—O2—Na1^{i}	58.2 (4)	Na2^{xii}—Mo1—O4—Na3	−22.58 (11)
O4—Mo1—O1—Na4^{ii}	−106.8 (4)	Na2^{xii}—Mo1—O3—Co1	128.5 (4)
O4—Mo1—O1—Na2^{v}	46.5 (3)	Na2^{xii}—Mo1—O3—Na4^{iii}	−89.6 (4)
Na1^{i}—Mo1—O4—Na3	100.90 (13)	Na2^{xii}—Mo1—O3—Na4^{ii}	−4.9 (3)
Na1^{i}—Mo1—O3—Na4^{iii}	112.1 (3)	Na2^{xii}—Mo1—O2—Na1	−93.4 (2)
Na1^{i}—Mo1—O3—Na4^{ii}	−163.2 (2)	Na2^{xii}—Mo1—O2—Na1^{i}	145.4 (2)
Na1^{i}—Mo1—O2—Na1	121.2 (7)	Na2^{xii}—Mo1—O1—Co1^{v}	132.8 (5)
Na1^{i}—Mo1—O1—Na4^{ii}	136.4 (5)	Na2^{xii}—Mo1—O1—Na4^{ii}	−153.3 (4)
Na1^{i}—Mo1—O1—Na2^{v}	−70.3 (4)	Na2—O6—C7—C1	77.9 (9)
Na1^{i}—O2—Mo1—Na4^{iii}	−30.3 (8)	Na2—O6—C7—O5	−106.1 (10)
Na1—O2—Mo1—Na4^{ii}	0.1 (8)	Na2^{ix}—O9—C9—O10	75.7 (9)
Na1^{i}—O2—Mo1—Na4^{ii}	−121.1 (6)	Na2^{xi}—O9—C9—O10	75.7 (9)
Na1—O2—Mo1—Na4^{iii}	90.9 (7)	Na2^{ix}—O9—C9—C5	−105.3 (8)
Na1—O2—Mo1—Na3	−151.1 (5)	Na2^{xi}—O9—C9—C5	−105.3 (8)
Na1^{i}—O2—Mo1—Na3	87.7 (5)	Na2^{xii}—O1—Mo1—O4	46.5 (6)
Na1—O2—Mo1—Na2^{v}	−93.4 (5)	Na2^{xii}—O1—Mo1—Na1^{i}	−70.3 (6)
Na1^{i}—O2—Mo1—Na2^{v}	145.4 (5)	Na2^{xii}—O1—Mo1—Na4^{iii}	127.4 (4)
Na1—O2—Mo1—O3	58.1 (6)	Na2^{xii}—O1—Mo1—Na4^{ii}	153.3 (6)
Na1^{i}—O2—Mo1—O3	−63.1 (7)	Na2^{xii}—O1—Mo1—Na3	25.4 (4)
Na1^{i}—O2—Mo1—O1	176.5 (5)	Na2^{xii}—O1—Mo1—O3	168.2 (4)
Na1—O2—Mo1—O1	−62.3 (6)	Na2^{v}—O1—Mo1—O3	168.2 (4)

Na1^{viii}—O8—C8—Na4^{xvii}	99 (3)	Na2^{v}—O1—Mo1—O2	−73.3 (6)
Na1—O8^{vii}—C8^{vii}—Na4	−111.7 (6)	Na2^{xii}—O1—Mo1—O2	−73.3 (6)
Na1^{xvii}—O8—C8—C3	100.5 (7)	O9—C9—C5—C4	−3.7 (12)
Na1^{viii}—O8—C8—C3	−49 (3)	O9—C9—C5—C6	171.2 (10)
Na1^{xvii}—O8—C8—O7	−81.3 (9)	C8—C3—C2—C1	−179.1 (9)
Na1^{viii}—O8—C8—O7	129 (2)	C8—C3—C4—C5	−179.9 (9)
Na1—O5—C7—O6	−113.2 (10)	O8—C8—C3—C2	164.4 (12)
Na1^{i}—O5—C7—O6	100.8 (10)	O8—C8—C3—C4	−18.1 (13)
Na1^{i}—O5—C7—C1	−83.5 (10)	C3—C2—C1—C7	175.3 (9)
Na1—O5—C7—C1	62.5 (11)	C3—C2—C1—C6	−3.9 (12)
Na4^{ii}—Mo1—O4—Na3	−106.3 (2)	C3—C4—C5—C6	1.8 (12)
Na4^{iii}—Mo1—O4—Na3	−154.44 (15)	C3—C4—C5—C9	176.6 (9)
Na4^{ii}—Mo1—O3—Na4^{iii}	−84.7 (3)	O7—C8—C3—C2	−13.8 (12)
Na4^{iii}—Mo1—O3—Na4^{ii}	84.7 (5)	O7—C8—C3—C4	163.6 (10)
Na4^{iii}—Mo1—O1—Na4^{ii}	−26.0 (2)	O10—C9—C5—C4	175.4 (10)
Na4^{ii}—Mo1—O1—Na2^{v}	153.3 (2)	O10—C9—C5—C6	−9.7 (11)
Na4^{iii}—Mo1—O1—Na2^{v}	127.35 (19)	C1—C2—C3—C4	3.4 (12)
Na4^{ii}—O3—Mo1—Na3	93.9 (4)	C1—C6—C5—C4	−2.3 (12)
Na4^{iii}—O3—Mo1—Na3	9.3 (7)	C1—C6—C5—C9	−177.3 (9)
Na4^{ii}—O3—Mo1—Na2^{v}	−4.9 (5)	C7—C1—C6—C5	−176.0 (10)
Na4^{iii}—O3—Mo1—Na2^{v}	−89.6 (5)	C2—C3—C4—C5	−2.4 (12)
Na4^{ii}—O3—Mo1—O2	−135.0 (4)	C2—C1—C7—O5	−179.5 (11)
Na4^{iii}—O3—Mo1—O2	140.3 (5)	C2—C1—C6—C5	3.2 (11)
Na4^{iii}—O3—Mo1—O1	−99.8 (5)	O5—C7—C1—C6	−0.3 (13)
Na4^{ii}—O3—Mo1—O1	−15.1 (4)		

Symmetry codes: (i) *x*, −*y*+3/2, *z*−1/2; (ii) *x*+1, −*y*+3/2, *z*+1/2; (iii) *x*+1, *y*, *z*; (iv) −*x*+2, −*y*+2, −*z*+1; (v) *x*, −*y*+3/2, *z*+1/2; (vi) −*x*+2, *y*−1/2, −*z*+3/2; (vii) −*x*+1, *y*+1/2, −*z*+3/2; (viii) −*x*+1, −*y*+1, −*z*+2; (ix) *x*−1, *y*, *z*; (x) *x*−1, −*y*+3/2, *z*−1/2; (xi) −*x*+1, −*y*+1, −*z*+1; (xii) −*x*+2, *y*+1/2, −*z*+3/2; (xiii) −*x*+2, *y*+1/2, −*z*+1/2; (xiv) *x*+1, −*y*+3/2, *z*−1/2; (xv) −*x*+2, −*y*+1, −*z*+1; (xvi) −*x*+2, *y*−1/2, −*z*+1/2; (xvii) −*x*+1, *y*−1/2, −*z*+3/2; (xviii) *x*−1, −*y*+3/2, *z*+1/2.